Nuclear Engineering and Design 106 (1988) 1–8
North-Holland, Amsterdam

MEASUREMENT OF MODE III FRACTURE ENERGY OF CONCRETE

Zdeněk P. BAŽANT [1] and Pere C. PRAT [2]

[1] *Professor of Civil Engineering, Center for Concrete and Geomaterials Northwestern University-Tech 2410, Evanston, Illinois 60208, USA*

[2] *Graduate Research Assistant, Center for Concrete and Geomaterials, Northwestern University, Evanston, Illinois 60208, USA*

Received 16 July 1987

The test specimens are cylinders with a circumferential notch, loaded in torsion. Maximum loads of geometrically similar specimens of sizes 1:2:4 are measured and Bažant's size effect method is used to determine from them the value of fracture energy for Mode III (antiplane shear). This value is found to be about three times larger than the Mode I fracture energy and about nine times smaller than the Mode II fracture energy measured before. These differences appear to be explicable by inclined tensile microcracks in the fracture process zone and a dependence of the fracture energy on the confining normal force across the fracture process zone.

1. Introduction

Shear failure is an important consideration for dynamic loading of various hardened structures and nuclear reactor vessels, as well as some ordinary types of beam or slab structures. In some of the failures observed, the fracture appears to take place in the shear mode or at least a combination of the shear mode and the opening mode, and so the failure analysis necessitates the value of the fracture energy for shear.

Shear fracture energy tests have been conducted by Bažant and Pfeiffer [7] with Mode II loading, i.e. in-plane shear loading. The present study presents the results of shear fracture tests in Mode III, i.e. the antiplane shear. A cylindrical specimen with a circumferential notch, subjected to torsion, is used for this purpose; see figs. 1 and 2.

2. Description of the experiments

Opposite couples were applied at the ends of the notched cylindrical specimen to produce a torque, T, as shown in figs. 1 and 3. To determine fracture energy by the size effect method [2,4,13], geometrically similar specimens of significantly different sizes were tested. The diameters of the cylinders were $d = 1.5$, 3, and 6 in. The length-to-diameter ratio was $l/d = 2$. A circular notch of thickness 1/16 in. was cast at mid-length perpendicular to the axis of the cylinder (figs. 1 and 2). The notch depth was $a_0 = d/4$.

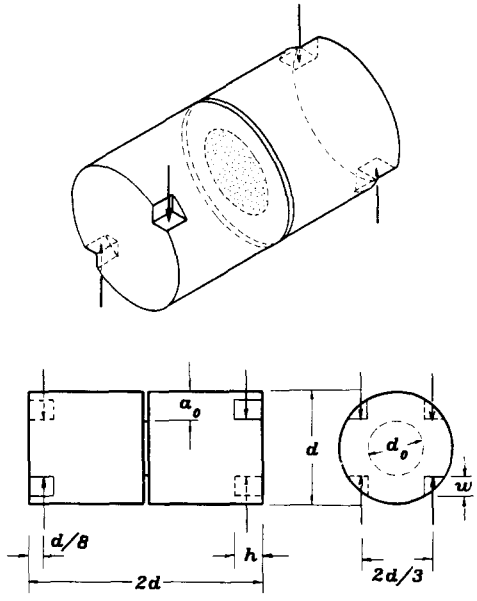

Fig. 1. Torsional circumferentially notched fracture specimens.

The torques were applied at each end as force couples in the way shown in figs. 1 and 3. The wedge-shaped cut-outs on which the loads were applied were formed in a standard cylinder mold using inserted pieces of wood treated against moisture absorption. The size and shape of the wedges are defined in fig. 1. Each end couple had an arm of $2d/3$ and was applied in a plane

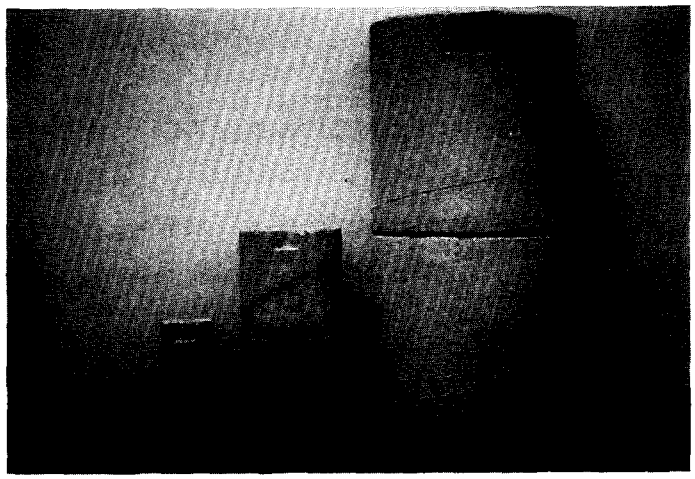

Fig. 2. Specimens of all sizes tested.

perpendicular to the axis of the specimens at a distance of $d/8$ from the ends.

Nine specimens were used, three for each size (fig. 2). Three companion cylinders for compression strength, 3 in. in diameter and 6 in. in length, were cast from the same batch of concrete as the fracture specimens of each test series. The mean and standard deviation of the compression strength f_c' after 28 days of moist curing are given in table 1. The 28-day f_c' values were not directly measured but calculated from the measured compression strength $f_c'(35)$ measured at the time of the tests at which the age of concrete was 35 days. The adjustment for age was based on the approximate formula [15] $f_c'(t) = f_c'(28)[1 + 0.277 \log(t/28)]$, from which $f_c'(28) \approx 0.974 f_c'(35)$.

The specimens were cast with the longitudinal axis in a vertical position, using water-cement ratio 0.6, and cement-sand-gravel ratio 1:2:2 (all by weight). The maximum gravel size was $d_a = 0.5$ in., and the maximum sand grain size was 0.19 in. The aggregate consisted of crushed limestone and siliceous Illinois beach sand (Lake Michigan). Portland cement C150, ASTM type I, with no admixtures and no air-entraining agents, was used.

The specimens were removed from the waxed cardboard molds after one day and were subsequently cured, until about one hour before the test, in a moist room at 95% humidity and 80°F temperature. The execution of the tests had to be postponed until the age of concrete was 35 days, instead of the standard 28 days, because a temporary malfunction of the testing equipment caused delay. Fig. 3 shows the specimens of all sizes installed in the testing machine. Fig. 4 exhibits the fractured specimens after the test showing the failure surface. The values of the strength and fracture energy given in this paper are all corrected from the measured values to obtain comparable values at 28 days.

All the tests were carried out at room temperature in a closed loop MTS machine under stroke-control condi-

Table 1
Compression strength of concrete used

a_0	f_c' (psi)	Std. dev. (psi)
$d/6$	5588	158
$d/4$	5633	221
All tests	5610	158

1 psi = 6.895 kPa.

Table 2
Maximum torque

Test		Maximum torque (lb·in.)			Average max. torque (lb·in.)
d	a_0	T_1	T_2	T_3	
6.0	1.00	10560	11520	10920	11000
6.0	1.50	6840	7020	6540	6800
3.0	0.50	1560	1524	1584	1556
3.0	0.75	936	984	966	962
1.5	0.25	213	219	216	216
1.5	0.38	140	132	128	133

1 lb·in. = 175 N·m.

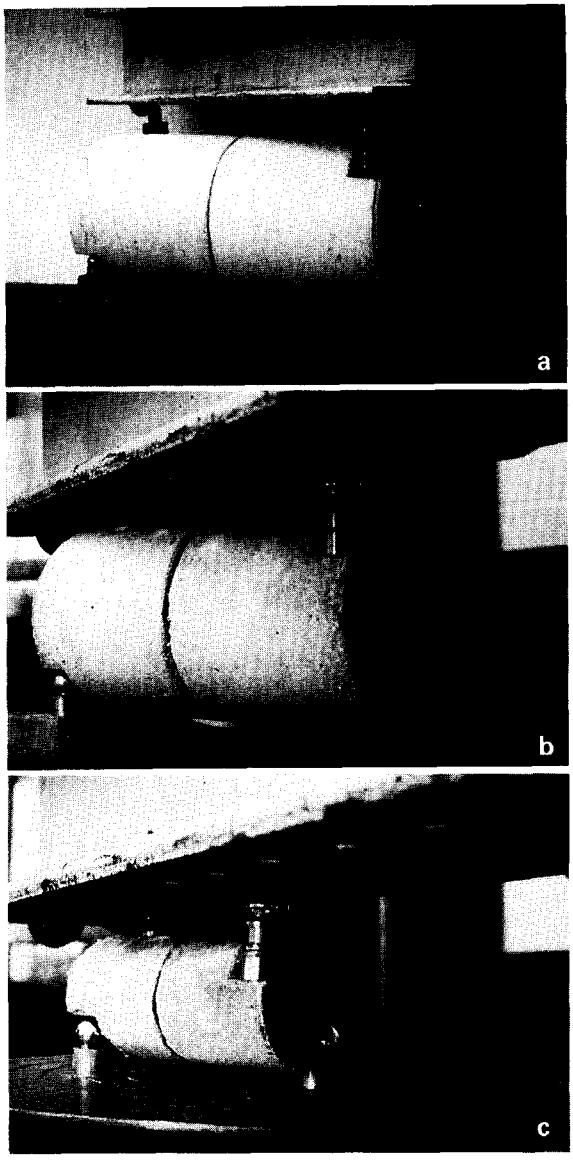

Fig. 3. Specimens during test and the loading arrangement: (a) large specimen ($d = 6$ in.); (b) medium specimen ($d = 3$ in.); and (c) small specimen ($d = 1.5$ in.).

tions. The loading rates were chosen such that the time to failure was 3 to 5 min for specimens of all sizes. To calculate the fracture energy from size effect analysis, one needs to measure only the maximum loads of the specimens of various sizes. The measured maximum torques T are given in table 2.

3. Size effect method for determining the fracture energy

The size effect is understood as the dependence of the nominal stress at failure τ_N on the characteristic dimension of the specimen, d, when geometrically similar specimens or structures are considered. For three-dimensional similarity, τ_N is generally defined as $\tau_N = CP/d^2$ where P = maximum load, d = characteristic dimension of the body, and C = arbitrary nondimensional constant. For the present specimens $\tau_N = 16T/\pi d^3 = CP/d^2$, where T = maximum torque, and $C = 16R/\pi d$ which is constant since R/d = constant for geometrically similar specimens ($T = PR$ where R is the arm of the force couple applied at the ends). Note that the value of C has no effect on the values of fracture energy given by eq. (3) which follows. The value of τ_N as defined represents the maximum elastic stress if there were no notch or crack.

Because the cracks in concrete propagate with a relatively large microcracking zone which blunts the fracture front, the size effect represents a transition between the plastic limit analysis, for which there is no size effect (i.e. τ_N is constant), and the classical linear elastic fracture mechanics, for which the size effect is the strongest possible and is of the type $\tau_N \sim d^{-1/2}$. This transition may be described by the approximate Bažant's size effect law

$$\tau_N = Bf_t' \left[1 + \frac{d}{\lambda_0 d_a}\right]^{-1/2}, \tag{1}$$

where B and λ_0 are empirical constants, d_a is the maximum size of aggregate, and f_t' is the tensile strength of concrete. Eq. (1) has been theoretically derived for three-dimensional problems in ref. [13], and for two dimensional problems in ref. [2] and more precisely in ref. [4]. It has been experimentally validated in Mode I (opening) fracture [7,12] and has also been found to approximately apply for Mode II (shear) fracture [3,7]. Tests further showed that eq. (1) is applicable to various brittle failures of concrete structures such as the failure of beams in torsion, the punching shear failure of slabs, the pull-out failure of steel bars embedded in concrete, etc. [6,8,9,10].

To determine parameters B and λ_0, eq. (1) may be transformed to the form:

$$\left[\frac{f_c'}{\tau_N}\right]^2 = \frac{1}{B^2\lambda_0}\frac{d}{d_a} + \frac{1}{B^2}. \tag{2}$$

Eq. (2) represents a linear relation between $(f_t'/\tau_N)^2$

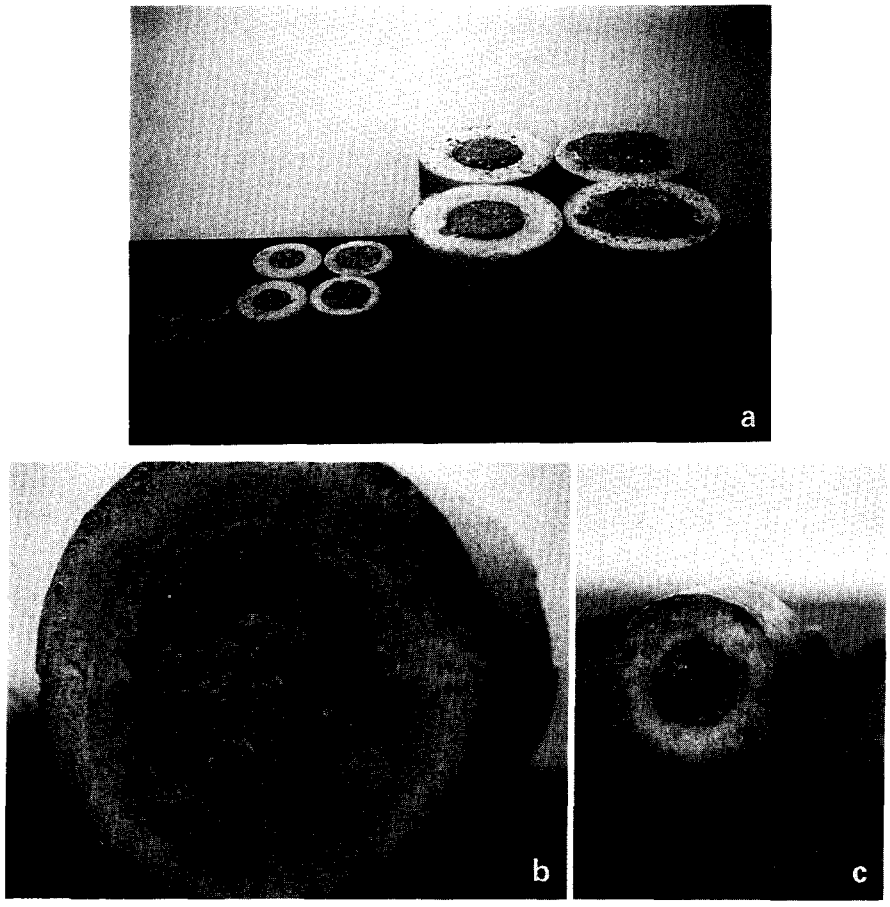

Fig. 4. Fractured specimens after the tests, showing the failure surfaces: (a) complete set of specimens; (b) detail of large specimen ($d = 6$ in.); and (c) detail of small specimen ($d = 1.5$ in.).

and d/d_a and may be rewritten as $Y = AX + C$ with $Y = (f_t'/\tau_N)^2$, $X = d/d_a$, $C = 1/B^2$, and $A = C/\lambda_0$. So the constants A and C may be obtained by linear regression of the test results, from which $B = C^{-1/2}$ and $\lambda_0 = C/A$. The regression plots also yield statistics of the errors. The coefficient of variation $\omega_{Y|X}$, and the correlation coefficient r are given in fig. 5.

As proposed by Bažant [4,13], the concrete fracture energy, G_f, may be uniquely defined as the energy release rate required for crack propagation in an infinitely large specimen. This definition must, in theory, yield results independent of both the size and the shape of the specimen, provided the correct size effect law for extrapolation to infinite size is known. The exact size effect law is unknown, but the approximate size effect law in eq. (1) was shown to be adequate for practical purposes. The following formula has been derived [5,11,13]:

$$G_f = \frac{g(\alpha_0)}{AE_c} f_t'^2 d_a \tag{3}$$

in which $\alpha_0 = a_0/r$; a_0 = notch depth; r = radius of the cylinder; E_c = modulus of elasticity of concrete; f_t' = direct tensile strength of concrete; $A = 1/B^2\lambda_0$ = slope of the regression line as already defined; $g(\alpha_0)$ = nondimensional energy release rate of the specimen according to the linear elastic fracture mechanics, which can be found for the basic specimen geometries in textbooks and handbooks, and can be in general determined by linear finite element analysis. For the specimens with the notch depth $a_0 = d/6$, $g(\alpha_0) = 1.57(1 + \nu) = 1.85$, and for the specimens with the notch depth

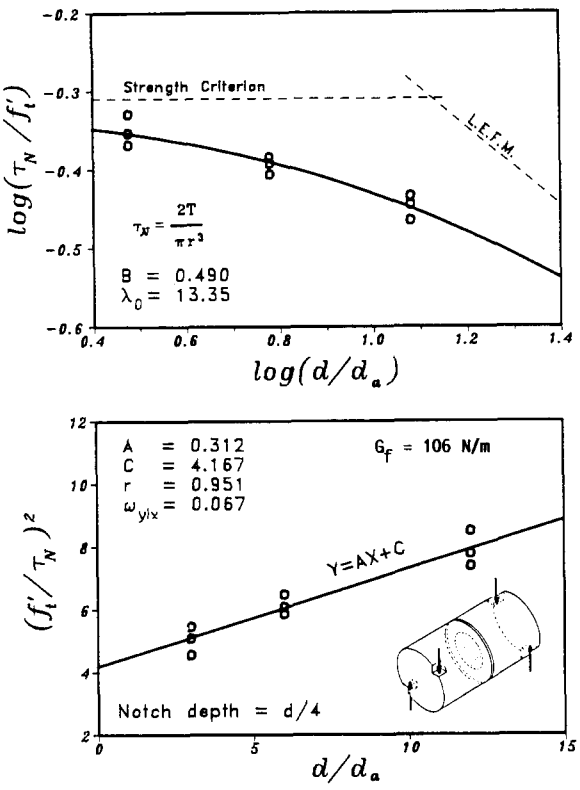

Fig. 5. Tests results: (a) size effect plots, and (b) linear regression plots.

$a_0 = d/4$, $g(\alpha_0) = 6.99(1+\nu) = 8.25$ [14,16]. These values, which are valid for Poisson ratio $\nu = 0.18$, have been used in all the calculations.

The tensile strength was estimated from the formula $f_t' \approx 6 f_c'^{1/2}$ where f_c' and f_t' are in psi, f_c' = compression strength. Since the slope A of the linear regression plots is proportional to $f_t'^2$, an error in f_t' has no effect on the fracture energy values.

The values of $\tau_N = 16T/\pi d^3$ calculated from the measured maximum torques T, are plotted in fig. 5. The plots at the top demonstrate that the measured τ_N agrees with the size effect law (shown as the solid curve) quite well. The plots at the bottom show the linear regression used to determine the mean values of the parameters of the size effect law.

The fracture energy values obtained in this manner correspond to the age of 35 days. They were then transformed to 28 days by using Bažant and Oh's empirical formula [1]:

$$G_f = (2.72 + 0.0214 f_t') f_t'^2 d_a / E, \tag{4}$$

which yields $G_f(28) = 0.976 G_f(35)$. Fig. 5 has been plotted using the 28 day values. The resulting fracture energy value, which represents the basic result of this study, is

$$G_f^{III} = 0.61 \text{ lb./in.}(106 \text{ N/m}). \tag{5}$$

For comparison, previous tests of essentially the same concrete yielded for Mode II and Mode I [7] the values:

$$\left.\begin{aligned} G_f^{II} &= 5.9 \text{ lb./in.}(1040 \text{ N/m}) \\ G_f^{I} &= 0.19 \text{ lb./in.}(33 \text{ N/m}) \end{aligned}\right\}. \tag{6}$$

4. Discussion of test results

Comparison with the Mode II and Mode I fracture energies (eqs. (5)–(6) shows a surprise. The values of G_f^{III} might have been expected to be about the same as G_f^{II} (and far larger than G_f^{I}). But this has not turned out to be the case. The measured G_f^{III} is much smaller than G_f^{II}. The mechanism which explains this finding will require further study. Since the present Mode III test achieves the shear fracture conditions better than the Mode II test, the meaning of the G_f^{II} values obtained previously calls for closer examination.

A clue is provided by the experimental observation that the results of shear fracture tests are very sensitive to the restraint of the specimen in the direction normal to the fracture plane (the axial direction of the cylinder for the present tests). In pilot tests prior to those reported here, it was discovered that very different results are obtained if friction at the supports is not eliminated. The confinement of the shear fracture zone due to the axial friction force, F, from the supports no doubt can raise the value of G_f significantly.

One series of pilot torsional tests of Mode III fracture was carried out with a different equipment – a large triaxial torsional testing machine which is very stiff because the test chamber (of 8.5 in. in diameter) is designed to resist chamber pressures up to 20000 psi plus axial forces up to 1100000 lb. The tests in this machine, which were made at essentially zero axial displacement at the ends of the cylindrical specimen, showed a different mode of failure, with a conical failure surface (see fig. 6). The axial force due to restraint in these tests was even capable of altering the failure mode, although the failure with a conical surface was still of the shear type.

To explain these observations, it is logical to assume that G_f^{III} as well as G_f^{II} is not a material constant but a

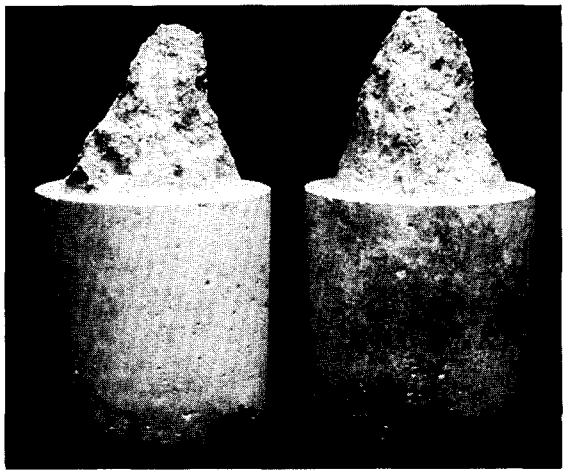

Fig. 6. Conical failure surface observed in previous tests of Bažant and Prat with stiff axial restraint.

material function $g(N_f)$ of the normal force N_f across the fracture process zone of length l_f, normal to the shear fracture plane, per unit length of the crack front edge. On the other hand, it may also be logical to assume that function $g(N_f)$ is the same for Mode II and Mode III shear fractures, i.e., for the same N_f, $G_f^{II} = G_f^{III} = G_f^s$ = shear fracture energy (regardless of the mode) such that

$$G_f^s = g(N_f), \tag{7}$$

where $g(N_f)$ is a function of N_f. The dimensions of G_f^s and N_f are the same, i.e. N/m.

That G_f^{II} must in general strongly depend on N_f has already been corroborated by Bažant and Pfeiffer's [7] finite element analysis of their Mode II fracture tests. Their study in fact made an even more general assumption, namely that both Mode I and Mode II fractures can be modeled by the same stress–strain relation for the fracture process zone. The reason one gets very different effective values of the fracture energy in Modes I and II can be found in the fact that in shear the microcracks in the fracture process zone do not lie in the fracture plane but are inclined to it by angle α (see fig. 7e,f). The column of intact material between adjacent inclined cracks carries compression force (F_c in fig. 7f). This force has an axial component (F_a in fig. 7f) which must be resisted together by the tensile stresses in the undamaged portions of the ligament (σ_1 in fig. 7a) and by the axial force F provided by the support. If axial displacements are prevented, the inclined compressive forces, F_c, are high and can offer a large resistance to shear. Hence the apparent values of fracture energy must be large. If the axial displacements are free, the inclined compression forces must vanish and thus cannot contribute to transmit shear stresses across the fracture process zone, and then the apparent value of shear fracture energy is small.

The action just described was automatically exhibited by a finite element model with a tensile softening stress–strain relation for the fracture process zone. Using such a model, Bažant and Pfeiffer [7] showed that the results of both Mode I and Mode II fracture tests can be matched with the finite element program using the *same* material properties. In this finite element analysis one does not directly use the fracture energy. Rather, one uses a triaxial stress–strain relation such that the area under the implied uniaxial tensile diagram equals G_f/w_c where w_c = effective width of the fracture process zone. This type of finite element analysis is planned to be carried out for the Mode III fracture tests in the subsequent stage of this shear fracture project.

As a crude approximate description of the role of the confining force N_f, we may write the longitudinal equilibrium condition assuming a zero axial resultant in the

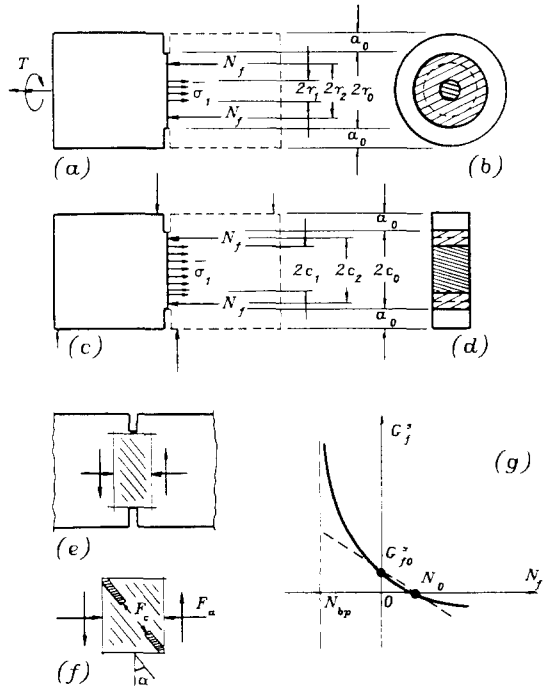

Fig. 7. Transverse stresses and inclined microcracking induced in the fracture process zone in shear fracture tests.

cross section (see fig. 7a, b). With the notation $\bar{\sigma}_1$ = average tensile stress in the tensile zone of the ligament and r_1 = radius of this zone, the equilibrium condition is $\pi r_1^2 \bar{\sigma}_1 = -2\pi r_2 N_f$ or $N_f = -\bar{\sigma}_1 r_1^2/2r_2$ where r_2 = radius up to the location of the compression force resultant N_f in the fracture process zone (fig. 7a). We may assume that $r_2 = k_2 r_1$ where k_2 = empirical constant of the order of 1 and $k_2 > 1$. Approximately we may write $\bar{\sigma}_1 = k_1 f_t'$ where k_1 = empirical constant of the order of 1, perhaps $k_1 = 0.5$ to 1.0, and f_t' = direct tensile strength of concrete. Solving for N_f, we get:

$$N_f = -\frac{k_1 f_t'}{2k_2} r_1. \tag{8}$$

For the previous Mode II fracture tests of Bažant and Pfeiffer [7], a similar equilibrium condition for the fracture plane cross section yields $2bc_1\bar{\sigma}_1 = -2bN_f$ or $N_f = -c_1\bar{\sigma}_1$ where b = specimen thickness, $2c_1$ = height of the tensioned portion of the ligament (fig. 7c,d). Setting again $\bar{\sigma}_1 = k_1 f_t'$, we get:

$$N_f = -c_1 k_1 f_t'. \tag{9}$$

Let us assume that function $g(N_f)$ can be approximated linearly (fig. 7g), i.e. $g(N_f) = G_0^s - c_f N_f$ where G_0^s = shear fracture energy at zero confining stress and c_f = nondimensional constant. For $N_f = l_f f_t'$ the fracture energy should become approximately zero, and so we have

$$g(N_f) = c_f(l_f f_t' - N_f). \tag{10}$$

Using eqs. (8) and (9) in eq. (10), we obtain

$$\frac{G_f^{II}}{G_f^{III}} = \frac{l_f + k_1 c_1}{l_f + r_1 k_1/2k_2}. \tag{11}$$

Since the fracture energy is defined for the limit case of an infinitely large specimen, we must assume $l_f \ll c_1$, $l_f \ll r_1$ and so

$$\frac{G_f^{II}}{G_f^{III}} = 2k_2 \frac{c_1}{r_1}. \tag{12}$$

According to the results of the tests made (eqs. (5)–(6)), $G_f^{II}/G_f^{III} \approx 9$. This value can be obtained from eq. (12) if it is assumed that $k_2 = 1.5$, $c_1 = 0.75c_0$, and $r_1 = 0.25c_0$ ($c_0 = r_0$). These values do not appear to be out of the range of the reasonably expected behavior. So we may conclude that the difference between G_f^{II} and G_f^{III} is not all that surprising and might be explicable by a rational theory. But further test as well as finite element studies will be required.

The previous analysis is based on the assumption of a linear dependence of G_f on N_f. In reality this dependence must be expected to be nonlinear. Materials such as concrete exhibit a brittle–ductile transition at a certain confining pressure p_{bd}; for ordinary concrete approximately $p_{bd} \approx 10\,000$ psi. Above this pressure value, there is apparently no softening and no fracture, and so $G_f^s \to \infty$. To satisfy this condition, the nonlinear dependence of G_f on N_f may be assumed in the form (fig. 7g),

$$G_f = A(N_f - N_{bd})^{-n} + B, \quad (N_f > N_{bd}), \tag{13}$$

where A, B, n = empirical positive constants and $N_{bd} = l_f p_{bd}$. Constants A and B may be determined from the conditions: (1) $G_f^s = 0$ for $N_f = l_f f_t'$, and (2) $G_f^s = G_{f_0}^s$ for $N_f = 0$ where $G_{f_0}^s$ = shear fracture energy at zero normal force across the ligament. This yields (see fig. 7g)

$$G_f^s = G_{f_0}^s \frac{(N_f - N_{bd})^{-n} - (N_0 - N_{bd})^{-n}}{(-N_{bd})^{-n} - (N_0 - N_{bd})^{-n}}, \tag{14}$$

where $N_0 = l_f f_t'$. This nonlinear form of the function $G_f(N_f)$ can considerably alter the values in eq. (12) which correspond to the observed ratio G_f^{III}/G_f^{II}.

The foregoing analysis has one weakness in the fact that the size effect law in eq. (1), which underlies the determination of fracture energy, might not be valid when the value of the normal force N_f across the fracture process zone is different for various sizes. If this were so, a more sophisticated extrapolation to infinite size would be required to obtain the fracture energy value. It remains to be seen whether this aspect can significantly affect the present results for the practical size range.

5. Conclusions

(1) The torsional circumferentially notched cylinder represents a relatively simple fracture test which yields consistent results and can be used to determine the shear fracture energy quite easily by Bažant's size effect method.

(2) Although according to the elasticity theory this specimen yields a perfect shear state (a stress field with antiplane symmetry near the crack front edge), it does not in general yield a perfect shear state for the actual material behavior. The reason is that transverse confining normal stresses are inevitably produced in the ligament cross section due to volume expansion caused by microcracking of the fracture process zone.

(3) The value of fracture energy obtained from the present Mode III tests is about 3-times larger than the Mode I fracture energy and about 9-times smaller than the Mode II fracture energy obtained with the double-notched four-point-loaded specimens used by Bažant and Pfeiffer [7].

(4) The discrepancies between the aforementioned Mode II and Mode III fracture energy values appear to be explicable by inclined microcracking in the fracture process zone, the associated volume change and the induced compressive force across the fracture process zone. As a result of this force, the shear fracture energy for Modes II and III (unlike the Mode I fracture energy) is not a material constant but must be considered to be a material function of the confining normal force.

Acknowledgements

The present research was supported by U.S. Air Force Office of Scientific Research under contract No. F49620-87-C-0030DEF with Northwestern University, monitored by Dr. Spencer T. Wu. Partial support for the experimental phase was also received under a cooperative research program with Universidad Politécnica de Madrid funded under a U.S.–Spanish Treaty (Grant CCA-8309071).

References

[1] Z.P. Bažant and B.H. Oh, Crack band theory for fracture of concrete, Matériaux et Constructions (Materials and Structures) RILEM, Paris, Vol. 16, No. 93 (1983) pp. 155–177.

[2] Z.P. Bažant, Size effect in blunt fracture: concrete, rock, metal, Journal of Engineering Mechanics, ASCE, Vol. 110, No. 4 (April 1984) pp. 518–535.

[3] Z.P. Bažant and J.-K. Kim, Size effect in shear failure of longitudinally reinforced beams, American Concrete Institute Journal, Vol. 81, No. 5 (1984) pp. 456–468.

[4] Z.P. Bažant, Fracture mechanics and strain-softening of concrete, Preprints, U.S.-Japan Seminar on Finite Element Analysis of Reinforced Concrete Structures, Japan Society for the Promotion of Science, Tokyo, May 1985, pp. 71–92.

[5] Z.P. Bažant, J.-K. Kim and P.A. Pfeiffer, Non-linear fracture properties from size effect tests, Journal of Structural Engineering, ASCE, Vol. 112, No. 2 (February, 1986) pp. 289–307.

[6] Z.P. Bažant and Z. Cao, Size effect in brittle failure of unreinforced pipes, ACI Journal, Vol. 83, No. 3 (May-June 1986) pp. 369–373.

[7] Z.P. Bažant and P.A. Pfeiffer, Shear fracture tests of concrete, Matériaux et Constructions (Materials and Structures), RILEM, Paris, Vol. 19, No. 110 (1986) pp. 111–121.

[8] Z.P. Bažant and P.C. Prat, Effect of Temperature and Humidity on Fracture Energy of Concrete, Report No. 86-12/692e (December 1986), Center for Concrete and Geomaterials, The Technological Institute, Northwestern University, Evanston, IL 60208, USA.

[9] Z.P. Bažant, S. Sener and P.C. Prat, Size effect tests of torsional failure of concrete beams, Report No. 86-12/428s (December 1986), Center for Concrete and Geomaterials, Northwestern University, Evanston, Illinois, 60208,USA.

[10] Z.P. Bažant and Z. Cao, Size effect in punching shear failure of slabs, ACI Materials Journal, Vol. 84, No. 1 (Jan.–Feb. 1987).

[11] Z.P. Bažant and P.A. Pfeiffer, Fracture energy of concrete: its definition and determination from size effect tests, ACI, Katharine and Bryan Mather International Conference on Concrete Durability, Vol. 1, Detroit 1987, pp. 89–109.

[12] Z.P. Bažant and S. Sener, Size effect in pullout tests, Report No. 87-5/428s (May 1987), Center for Concrete and Geomaterials, The Technological Institute, Northwestern University, Evanston, Il 60208, USA.

[13] Z.P. Bažant, Fracture energy of heterogeneous materials and similitude, Preprints, International Conference on Fracture of Concrete and Rock, edited by S. Swartz, Society for Experimental Mechanics, Inc., Houston, Texas, June 17–19, 1987.

[14] J.P. Benthem and W.T. Koiter, Asymptotic approximation to crack problems, Chapter 3 in: Methods of Analysis of Crack Problems, ed. by G.C. Sih (Jan. 1972, Noordhoff Int. Publ.).

[15] A.M. Neville, Properties of Concrete (Pitman Publishing Limited, London, 1981) Third Edition.

[16] H. Tada, P.C. Paris and G.R. Irwin, The Stress Analysis of Cracks Handbook (Del Research Corp., Hellertown, Pa., 1973).